Concept for an onshore tower structure made of UHPFRC segments for wind turbines

Traian-Nicu Toader [*1,2], Daniel Schmeer[1], Werner Sobek[1,3]

[1] *Universität Stuttgart, Institut für Leichtbau Entwerfen und Konstruieren (ILEK). Pfaffenwaldring 7 + 14, DE 70569, Stuttgart, Germany*
[2] *Technical University of Cluj-Napoca, Faculty of Civil Engineering, Department Structures. 15 Daicoviciu Str., RO 400020, Cluj-Napoca, Romania*
[3] *Werner Sobek Group GmbH. Albstraße 14, DE 70597, Stuttgart, Germany*

Abstract

Germany's decision to replace fossil fuels with renewable energy, made by the Federal Government, will require considerable innovations in almost the entire energy industry to achieve the goal in the shortest time [1]. One solution the present paper considers is an increase for energy generated by onshore wind turbines (WT) on complex mountainous terrain. In order to use these difficult areas for erecting new WT, the components for the plant need to be adapted or newly developed. One possible option is the development of new tower structures for onshore WT made of ultra-high performance fiber-reinforced concrete (UHPFRC) segments. The present paper focuses on the design concept and the dimensioning of innovative tower structures for onshore WT placed in the demanding conditions of the complex mountainous terrain. This structural concept in combination with UHPFRC leads to high material savings of up to 50% compared to existing solutions.

Rezumat

Decizia Statului Federal German de a înlocui producția de energie electrică bazată pe combustibili fosili cu cea bazată pe resurse regenerabile va necesita inovații considerabile, efectuate în cel mai scurt timp, în aproape întreaga industrie energetică [1]. Una dintre posibilele soluții ale aceastei probleme este prezentată în articolul de față ca fiind creșterea cantității de energie electrică produsă folosind turbine eoliene (WT) onshore amplasate în zone cu relief muntos complex. În vederea utilizării acestor zone de relief în scopul producției de energie electrică, este necesar ca părțile componente ale fermelor eoliene să fie adaptate sau reproiectate. Soluția propusă constă în proiectarea de noi turnuri pentru WT onshore alcătuite din segmente din beton de ultra-înaltă rezistență armat cu fibre disperse (UHPFRC). În articolul științific prezent accentul cade pe proiectarea conceptului structural și dimensionarea structurii prefabricate pentru turnuri de WT onshore amplasate în condițiile speciale ale ținuturilor cu relief muntos complex. Conceptul structural ales și împreună cu utilizarea UHPFRC, conduc la economii de material de cca. 50% în comparație cu soluțiile folosite curent în industrie.

1. Introduction

The use of tubular towers made of steel, concrete or hybrid steel–concrete has become standard in the wind energy industry. However, more powerful wind energy generators are leading to the need for installing the towers in regions with a complex mountainous terrain. This implies rethinking of existing solutions for the support onshore structure composed of tower and foundation, including design concept, life cycle and environmental repercussion. The need for transportation of larger prefabricated elements and more complex processes of assembling on site become important issues [2].

The concept of a segmented tower structure made of UHPFRC with external post-tensioned tendons was developed at the Institute for Lightweight Structures and Conceptual Design (ILEK) of the University of Stuttgart [3]. The unique mechanical properties of UHPFRC (with higher compressive strength of 150 to 250 MPa and higher fatigue resistance [4] than normal or high strength concrete) allow for the production of extremely slender and lightweight tower structures. Consequently, the reduction of the tower's own weight will result in material and energy savings [3]. Furthermore, the use of UHPFRC segments, in combination with external post-tensioned tendons, represents a highly promising economic alternative to steel tower structures.

The aim of the authors' research is to develop an alternative tower concept made of UHPFRC precast segments. The segmented structure is expected to meet the requirements of a WT and the acting external loads. The main focus of the current research is the design of a tower concept with a minimum weight and a reduced segmentation for an uncomplicated assembly on site.

2   Description of the tower concept

The technical solution of the tower concept is, on the one hand, material-related; on the other hand, it is orientated towards easy transport of the segments as well as fast and simple assembly and disassembly of the tower.

UHPFRC is distinguished by excellent material properties in terms of compressive strength and durability. In consequence, it is an ideal material for low-maintenance and structurally optimized towers for WT. For their investigations, the authors used ultra-high performance concrete with steel fiber reinforcement from the company Lafarge (namely Ductal®). Numerous experimental material-related investigations (approx. 150) were carried out to determine the material properties [3]. Table 1 summarizes the obtained mechanical properties with their characteristic values considering a 5% fractile value [3].

Table 1: Determined material properties on Ductal®, a Lafarge product [3]

Mechanical property	Characteristic value
Characteristic compressive cylinder strength, f_{ck}	183,8 MPa
Characteristic axial tensile strength without fiber orientation, $f_{ctk,el}$	7,7 MPa
Characteristic axial tensile strength with fiber orientation, $f_{ctk,1D,el}$	22,7 MPa
Secant modulus of elasticity, E_{cm}	59364 MPa
Compressive strain at the peak stress f_{cm}, ε_{c1}	4,0 ‰
Tensile strain corresponding the tensile elasticity limit, $\varepsilon_{ct,el}$	1,9 ‰

The production of high performance building components requires a proper quality control concerning homogeneous material distribution in the formwork, fiber orientation and thermal treatment. Therefore, such production prerequisites are more easily met in a plant rather than on site. This results in the need for segmenting the tower structure. Compared to the in-situ concrete construction, prefabricated segments can have further advantages; for instance, the production planning is not affected by weather conditions and, in addition, good productivity can be achieved through a high degree of prefabrication and fast assembly on site. However, the segments' size and weight is influenced by the means of transport, making the geometric restrictions of the finished parts as well as the joining type of the individual segments important.

The tower assembly consists of stacking truncated conic shape segments with horizontal dry joints and centrically post-tensioned tendons. The external tendons are placed outside the wall and on the inner side of the ring cross section, thus facilitating a minimized wall thickness for the segments. Therefore, the cross section can be optimized in accordance with the stress state, and there is no requirement for a minimum wall thickness in comparison with internal tendons. The external tendons can be easily installed and inspected, and, when necessary, re-tensioned or replaced.

If the tendons are unguided over the full height of the tower, then the tendons on the windward side coincide with the chord, Fig. 1 (a). The tendons on the leeward side touch the inside of the tower shaft [5]. The eccentricities of the tendons need to be considered for the design in the deformed state of the structure. However, their positioning was improved by introducing corbels on the inside of the tower shaft in such a way that the tendons follow a polygonal line in the deformed load-bearing structure without touching the inside of the tower shaft [5], Fig. 1 (b). This results in restoring forces and change-of-direction forces, for which the corbels must be designed.
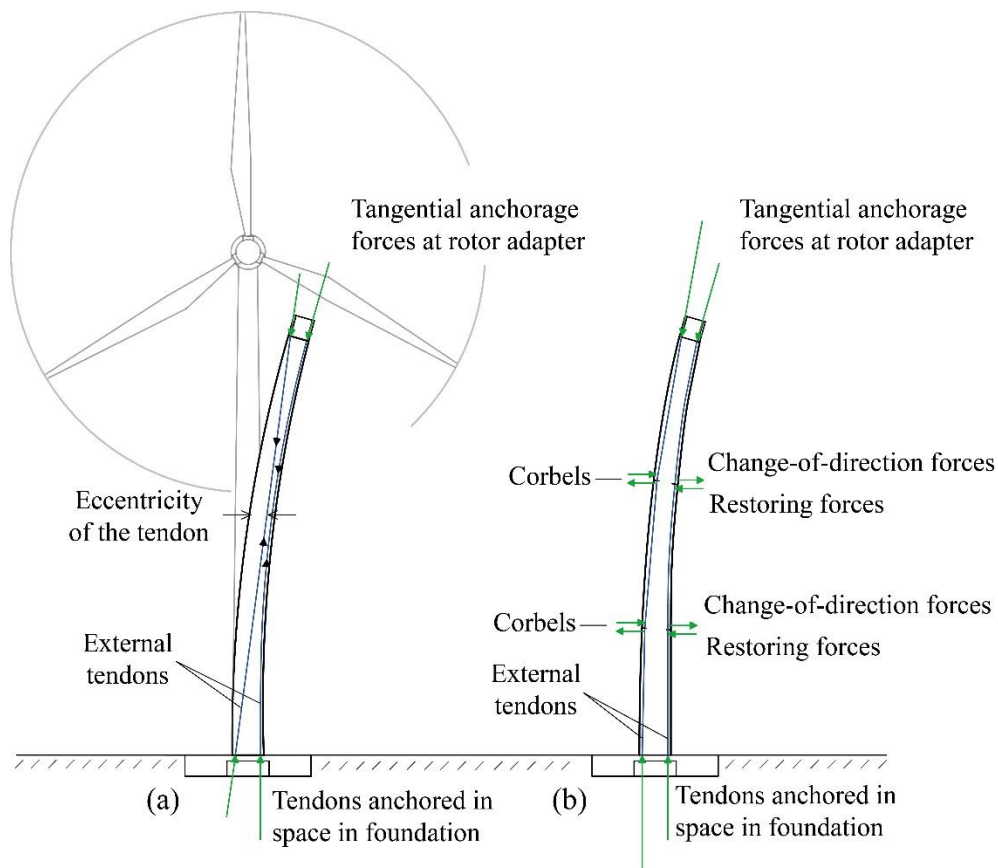
Figure 1. Deformed tower with external prestressing with (a) actions of exposed external prestressing tendons and (b) actions of corbel-guided staged tendons [6], [5] modified.

An exemplary design of an on-shore tower structure for WT in complex terrain is shown in Fig. 2. The tower shaft measures 72 m, has a base diameter $\varnothing_{TB} = 5$ m and a top diameter $\varnothing_{TT} = 3$ m. A steel adapter is fixed to the topmost concrete segment enabling the rotor to be connected to the tower. The tower segmentation consists of truncated conical rings with heights of 3,6 m (10 pieces) respectively, 18 m (2 pieces). The overall size of the segments was chosen considering the permissible transport dimensions according to [6]. The segments have an overall constant wall thickness of 100 mm. This thickness results out of a preliminary design taking into account the natural frequencies of the tower and the Campbell diagram corresponding to a Fuhrländer FL600 model with a capacity of 0.6 MW.
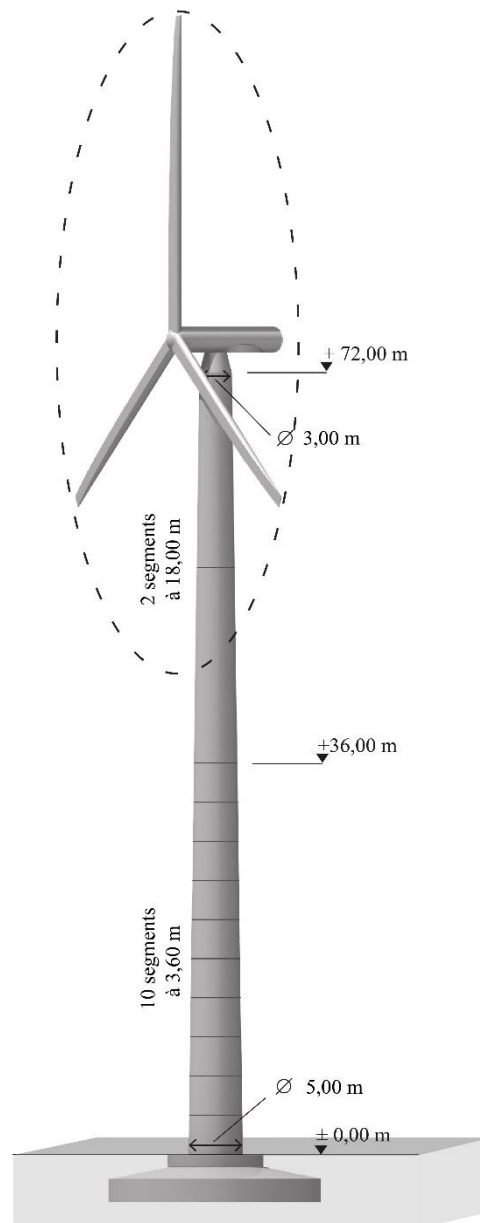
Figure 2. Preliminary design of an onshore segmented tower of UHPFRC for WT [8].

A concept for assembling the precast segments is illustrated in Fig. 3. In the joining region, the annular segments are provided with a toothed strip. The geometry of the joint allows the transfer of reaction forces from one segment to another through compression-only joints. The geometry and the load bearing capacity of the dry joint were extensively studied in [3].

The external tendons are guided inside the tower shaft by guiding corbels at defined intervals. This overcomes the eccentricity of an unguided external tendon described above. Two types of corbels can be distinguished, one with a rectangular cross-section, which solely take over the guidance of the tendons, and more voluminous ones with a trapezoidal cross-section, meant for anchoring the tendons.

guidance of tendon

anchorage of tendon

1 guiding corbel
2 tendon
3 segment made of UHPC
4 scaling
5 dry joint
6 tendon anchorage
7 anchoring corbel

joint geometry

$\alpha = 20°$
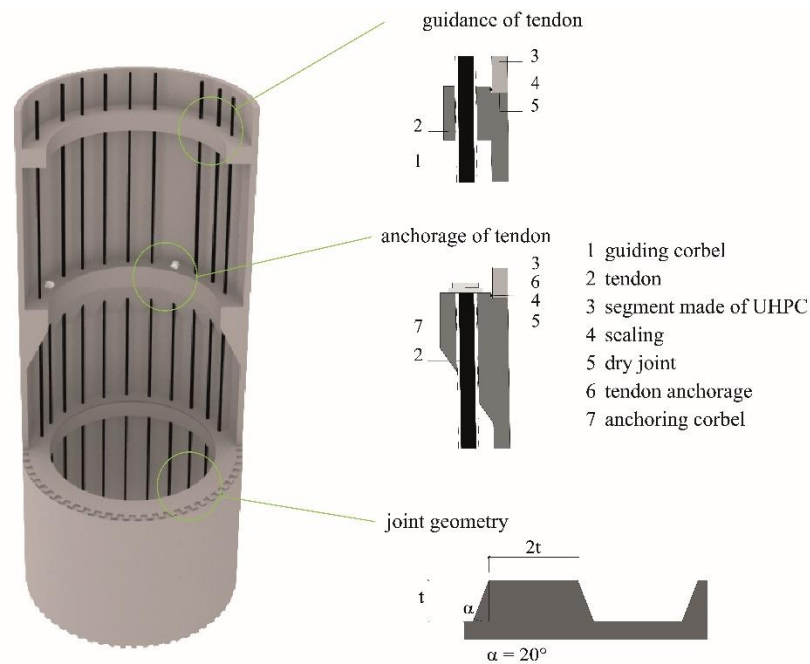
Figure 3. Connecting the segments by means of dry joints and external post-tensioning [7].

3. Preliminary design of the tower structure

In general, the design takes into account multiple loads: self-weight of the tower, dead load of the WT and installations [5], actions due to the operation of the turbine, wind loads, thermal actions, icing up of structural elements, earthquakes, corrosion and erosion [9]. The preliminary design is based on an eigenfrequency analyse to develop the tower geometry with its stiffness and mass in such a way that the resonance effect due to the WT action is avoided.

3.1 Wind turbine

In determining the reaction forces of the WT upon the tower it is necessary to take into account the particularities of the rotor-nacelle and of the control engineering system. The relevant technical data of the WT used are given in Table 2. Because the WT is excited periodically (e.g. by blade passing and oblique inflow) as well as infrequently (e.g. by wind turbulences and earthquakes), the supporting structure is highly dynamically loaded [10]. In the case of resonance, this can lead to a failure of the load bearing system. Therefore, it is imperative to avoid the natural frequency of the structure falling in the range of the rotor and blade excitation frequencies. This results in the admissible frequency ranges shown on the Campbell diagram, Fig. 4. The purpose of the Campbell diagram is to visualize the relation between the first eigenfrequency f_1 of the structure and the excitation frequency of the rotor. In the diagram, the rotor frequency f_R (1P excitation) and the blade passing frequency f_E (3P excitation for a three-bladed wind turbine) are plotted against the rotational speed of the rotor with a scatter of ±10 % [11]. The grey area indicates the range in which the rotor of the WT operates. As a result, three design ranges can be identified when considering the dynamic behaviour of a WT [12], [13]: "soft-soft", "soft-stiff" and "stiff-stiff". If the tower's natural frequency is above the 3P excitation, the design is called "stiff-stiff". Although this does not

involve a resonance risk, an enormous use of material is necessary to achieve high stiffness for tall towers. As a consequence, a "stiff-stiff" design will neither lead to a weight-minimized structure nor to an economical solution. A "soft-soft" design leads to a natural frequency below the 1P excitation. This design is excluded primarily because of the danger brought by ordinary wind speeds for which the rotor excitation will lead to tower oscillations with large amplitudes. Moreover, a tubular concrete structure with an excessively thin wall will lead to local stability losses and local material failure. Consequently, excluding the "soft-soft" and "stiff-stiff" ranges, a "soft-stiff" design, between the periodic excitation of 1P and 3P, proves to be the most suitable design domain for the tower shaft. The permissible natural frequency of the tower is set between 0,505 and 0,585 Hz, Fig. 4.

Table 2: Technical data of the WT model – Fuhrländer FL600 [14]

Rated power	600 kW
Rotor diameter	50 m
Maximum hub height	75 m
Nominal speed range	13 – 27 U/min
Total weight (rotor + hub + nacelle)	35 to
Vertical eccentricity of the rotor's midpoint	3,0 m
Horizontal eccentricity of the rotor's midpoint	1,8 m
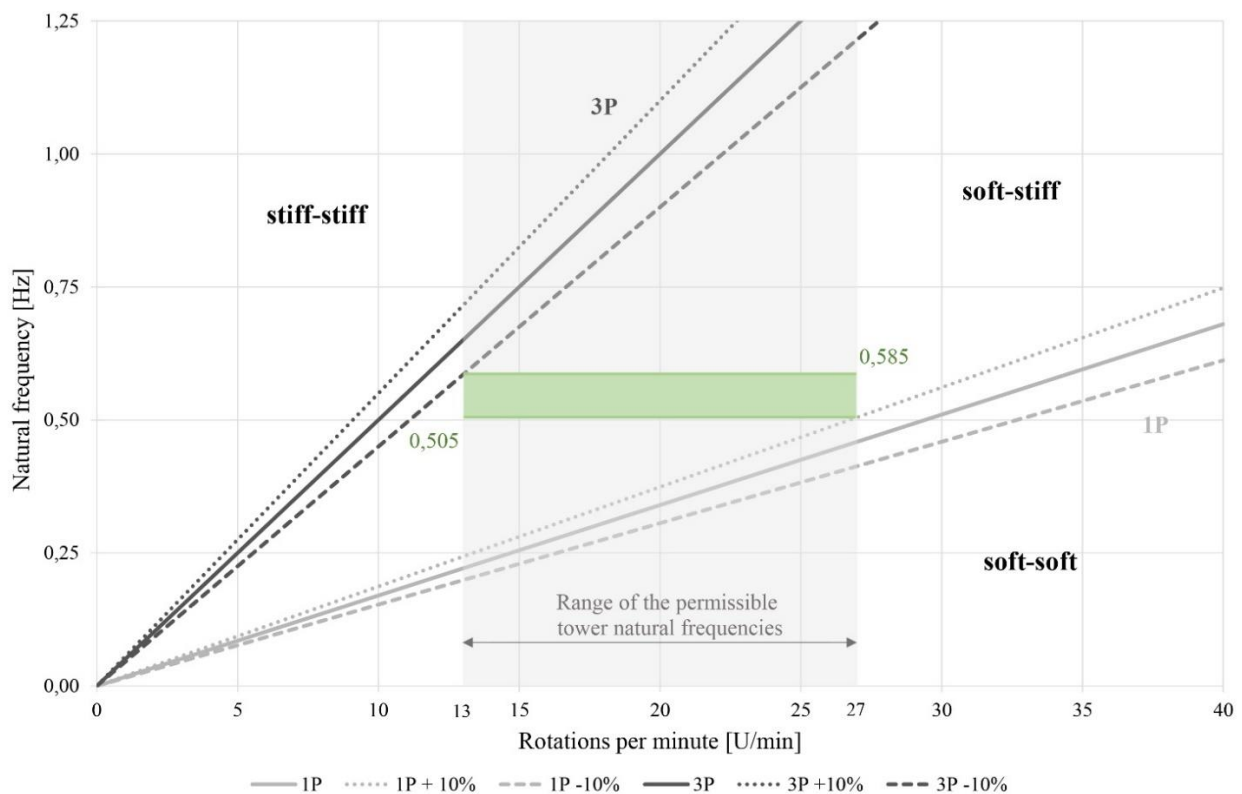
Figure 4. Campbell diagram of a FL600 wind turbine and the range of permissible tower natural frequency.

3.2 Foundation

Besides the chosen UHPFRC and the given WT, the pre-dimensioning of the tower shaft was influenced by the characteristic values of the building ground and the type of foundation. The possible tower geometry (height, diameter and wall thickness) was initially restricted by considering a minimum and maximum foundation stiffness. The aim of such an approach was to determine a range of different tower diameters with varying wall thicknesses, independently of the exact soil and foundation parameters. Based on a parametric study in terms of natural frequency, the range for the tower's possible geometry was determined.

The calculation was based on a multi-mass oscillator conservative model, neglecting the effects of structural damping and aerodynamic damping on the natural frequency [15]. By solving the eigenvalue problem, the eigenfrequency of the multi-mass oscillator model was determined, Eq. (1):

$$\det(\overline{K} - \omega_i^2 \cdot \overline{M}) = 0 \tag{1}$$

where $\overline{K}$ is the stiffness matrix, $\overline{M}$ is the total mass and ω_i is the "i" natural frequency of the multi-mass oscillator model.

The parametric design was made for two degrees of foundation soil stiffness corresponding to cohesive soils (clay, semi-hard to hard) and rocks (layered and brittle). This assumption was made in order to cover the whole range of possible degrees of foundation soil stiffness. Based on the soil's mechanical properties and the loads acting upon the tower, a circular raw foundation with a diameter of 14 m was chosen. Thus, the minimum and maximum equivalent spring stiffness for translation and rotation were calculated using Eq. (2) and (3), according to [16]:

$$k_u = \frac{8 \cdot G_d \cdot r_0}{2 - \nu} \tag{2}$$

$$k_\varphi = \frac{8 \cdot G_d \cdot r_0^3}{3 \cdot (1 - \nu)} \tag{3}$$

where G_d is the dynamic shear modulus [MN/m^2], r_0 is the foundation's radius [m] and ν is the Poisson ration. The required soil dynamic properties G_d and ν were chosen according to [17]. Further on, the spring constants characterizing the considered range of soil types are summarized in Table 3.

Table 3: Spring constants of the considered soil types [7]

Type of soil	k_u [MN/m]	k_φ [MN·m/rad]
Cohesive soil (clay, semi-hard to hard)	2.715 – 10.839	112.574 – 498.909
Rock (layered, brittle)	30.270 – 160.000	1.076.078 – 6.097.777

3.3 Natural frequency analysis

The calculations of the natural frequency are based on a 3-dimensional multi-mass oscillator model consisting of the WT mass with its eccentricities, the UHPFRC tower's own mass and the foundation. The multi-mass oscillator model is an example of a "lumped mass" approach. The tower was defined as a line object with several point masses. Due to the centrical prestressing and the horizontal guidance of the tendons through the corbels, the prestressing has no influence on the natural frequency [5]. The structure-soil interaction was modelled using translational springs (k_u)

and rotation springs (k_φ). The foundation spring stiffness was determined in respect to the type of foundation, size of foundation and the soil type characteristics. The numerical simulations for determining the tower's natural frequency consisted of a parametric study of the wind tower structure using the SAP2000 finite element software. These results were checked with analytical models. Therefore, static and dynamic analyses were performed taking into account the second order effects (P-Δ). Fully closed dry joints in the ultimate limit state (ULS) were considered for the model, so that the lateral bending stiffness of the tower is not reduced because of the segmentation. The parameters in the analysis are: the base diameter of the tower, the wall thickness of the segments, the stiffness of the foundation-soil system and the magnitude of the prestress force. In total, a set of 48 parameterized models were used.

The data generated by this parametric study are reported in Fig. 5, in the hypothesis of a site with cohesive soil. The possible towers have a base diameter of between 4 and 8 m and a constant wall thickness along the tower height of 50 mm to 300 mm. The graph shows that the first natural frequency increases significantly together with the wall thickness from 50 to 100 mm. For thicker wall values of up to 300 mm, there is only a minor increase in the first natural frequency. Based on the permissible frequency range of the "soft-stiff" design, the tower`s possible geometry was limited. On the whole, the base diameter of the shaft can take values between 4 and 5 m and wall thicknesses of 75 up to 300 mm in respect to the chosen diameter.
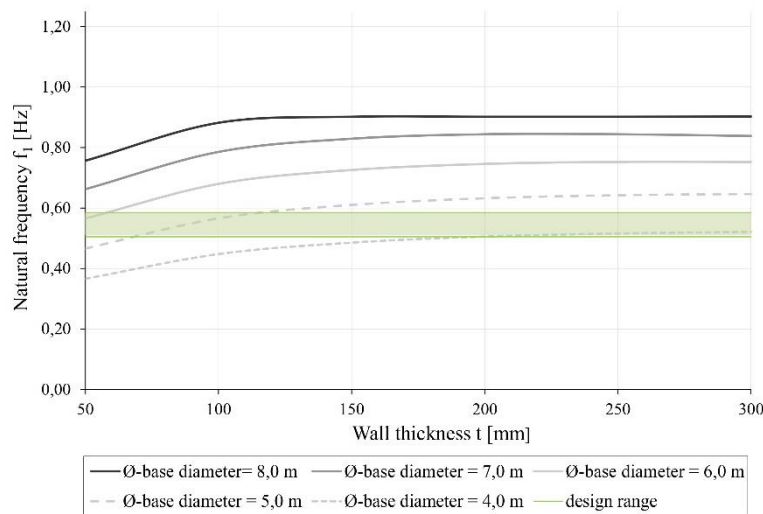
Figure 5. The tower's first natural frequency depending on various wall thicknesses and base tower diameters, considering the foundation on cohesive soil
(k_u = 2.715 MN/m and k_φ = 112.574 MN·m/rad.

Similarly, the permissible geometry of the tower was also determined for foundations placed on rock, Fig. 6. It can be seen that the first natural frequency characterizing each tower configuration increases for all base diameters once the wall is thickened. The base of the tower can be limited to a size of 5 m in diameter and wall thicknesses between 60 and 100 mm. Whereas for a base diameter of 4 m the permissible wall thickness varies between 150 and 300 mm.
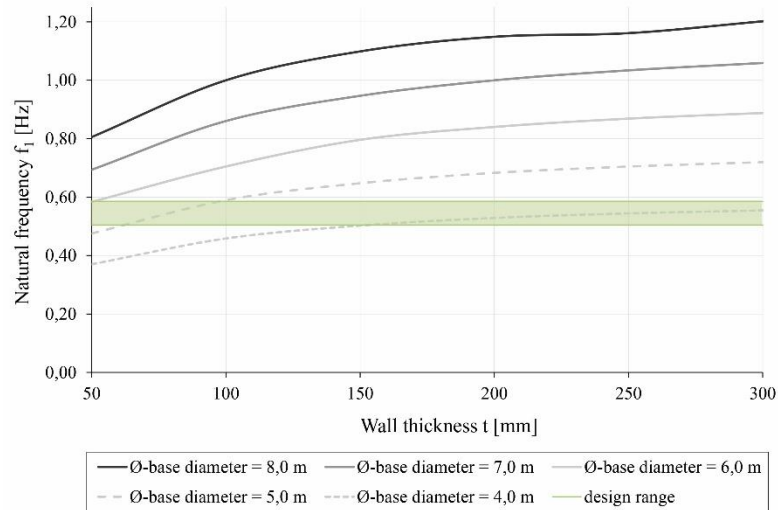
Figure 6. The tower's first natural frequency depending on various wall thicknesses and base tower diameters, considering the foundation on rock (k_u = 160.000 MN/m and k_φ = 6.097.777 MN·m/rad).

Finally, the range of permissible geometry was combined from both types of ground, and so the design of the tower structure became independent of the stiffness of the foundation-soil system. Consequently, a wide variety of configurations can be selected between tower diameter and wall thickness. Possible tower structures considering their use of material are listed in Table 4. This shows a high potential of the tower concept with mass savings up to 50% compared to existing towers [18].

Table 4: Possible geometry of the tower and its material consumption [7]

Height l [m]	Tower diameter		Wall thickness t [mm]	Volume V [m³]
	$\varnothing_{TB}$ [m]	$\varnothing_{TT}$ [m]		
72	5	3	100	˜120
72	4	3	200	˜175
72	4	3	300	˜210
72	4	3	300	˜240

4. Dimensioning of the tower structure

Starting from the results of the pre-dimensioning, the tower geometry was dimensioned and weight optimised. The wall thickness was modified in order to cover the maximum stresses in the relevant load combinations and the prestressed force was calculated as the minimum necessary force.
The numerical model was updated with the final geometry of the tower. It has a base diameter of 5 m and the segment wall thickness varies from the bottom to the top, from only 130 mm to 100 mm and 60 mm. Nevertheless, the natural frequencies of this tower stays between 0,543 and 0,567 Hz, which fits in the allowed range (Fig. 4).

4.1 Design situations and load cases

During the utilisation period of an onshore tower structure for WT there are several representative actions. For dimensioning purposes, a set of design situations was identified to cover the most significant conditions that the structure may experience. The design load cases (DLCs) were determined from a combination of specific transport, assembly, operation and maintenance design

situations [19]. Performing the structural analysis requires identifying the proper DLC group for each design situation for which the partial safety factors are to be extracted, Table 5. Depending on the action frequency and its nature, there are four DLC groups: normal and extreme actions (N), accidental actions (A), temporary actions during transport and erection (T), as well as permanent actions leading to material fatigue (F). Due to lack of data for several DLCs and the large number of possible load combinations, only the DLCs framed in a box from Table 5 were considered. Therefore, in the numerical simulations the following wind conditions were taken into account: normal turbulence model (NTM) in the production mode (1.0, 1.1 and 1.2), extreme operating gust (EOG) in the production mode (1.6) and extreme wind speed model (EWM) in the parked state (6.1). The appropriate partial safety factors for each DLC were identified depending on the DLC group in accordance to the DIN EN norm series and their national annexes, Table 6.

Table 5: Design load cases [19]

Design situation	DLC	Wind conditions	DLC group
Power production	1.0	NTM	N
	1.1	NTM	N
	1.2	NTM	F
	1.3	ECD	N
	1.4	NWP	N
	1.5	EOG_1	N
	1.6	EOG_{50}	N
	1.7	EWS	N
	1.8	EDC_{50}	N
	1.9	ECG	N
	1.10	NWP	F
	1.11	NWP	N
	1.12	NWP	A
Power production plus occurrence of fault	2.1	NWP	N
	2.2	NWP	A
	2.3	NTM	F
Start-up	3.1	NWP	F
	3.2	EOG_1	N
	3.3	EDC_1	N
Normal shut-down	4.1	NWP	F
	4.2	EOG_1	N
Emergency shut-down	5.1	NWP	N
	5.2	NWP	A
Parked (standstill or idling)	6.0	NWP	N
	6.1	EWM	N
	6.2	EWM	A
	6.3	EWM	N
	6.4	NTM	F
	6.5	EDC_{50}	A
	6.6	NWP	N
Parked plus fault conditions	7.1	EWM	A
Transport, erection, maintenance and repair	8.1	To be specified by the manufacturer	T
	8.2	Vortex-induced transverse vibrations	F

Table 6: Partial safety factors γ_F according to DIBt guideline [19]

Action	DLC group			
	N	**A**	**T**	**F**
Unfavorable permanent loads	1,35	1,10	1,25	1,00
Favorable permanent loads	1,00	1,00	1,00	1,00
Prestress	1,00	1,00	1,00	1,00
Wind loads	1,35	1,10	1,50	1,00
Operational forces	1,35	1,10	1,50	1,00
Thermal actions	1,35	-	-	1,00
Earthquake	-	1,00	-	1,00

4.2 Ultimate limit state (ULS)

Structures must be able to withstand all possible actions with sufficient reliability, regardless of the material and type of design used, and must also meet the required performance characteristics in the ULS. Therefore, the results of the analyses were extracted and compared with the resistance of the components [20]. In the present limit state, the upper limitation of the concrete compression stresses and the checking for decompression are decisive for the structural design.

The check for decompression was used in the hypotheses of a design with fully closed joints. This way the overall stiffness of the tower structure remained unchanged. To ensure this condition, the prestressing force $P_{m\infty}$ at the time $t = \infty$ must be chosen in such a way that no tensile stresses occur in the joint regions. The equation for determining the stress at the outer point in a certain cross section of the tower is:

$$\sigma_{Ed} = -\frac{|N_{Ed}| + \gamma_P \cdot |P_{m\infty}|}{A_{cs}} + \frac{M_{Ed} + \Delta M_{II}}{W} < 0 \tag{4}$$

The results for the necessary applied prestress force, P_{m0} are shown in Table 7. This takes into account the time-dependent stress force losses due to creep and shrinkage of the concrete and relaxation of the steel tendons. These stress force losses are set at 12,5 %, a value proposed by [3] for UHPFRC with posttensioning. In accordance with the necessary prestressing force distribution along the height of the tower (Table 7), the tendons are anchored in three sections at 28,8 m, 54,0 m and 72,0 m altitude. For economic reasons, the type „VT-CMM KD" was chosen and the necessary number of tendons was calculated so that each tendon is maximally utilized.

Below are summarized the results of the global analysis with decompression in each joining section checked. The calculated amount of tendons in the base third of the structure is 24, with eight wires each, and a cross section area per wire of 165 mm^2. Due to the geometry restrictions of the door opening, 23 tendons with eight (4 by 2) wires each and another two tendons near the door edges with four (2 by 2) wires are chosen, Fig. 7. In the middle third just 16 tendons are needed due to the smaller bending moments. While in the top third, the structure requires eight tendons.
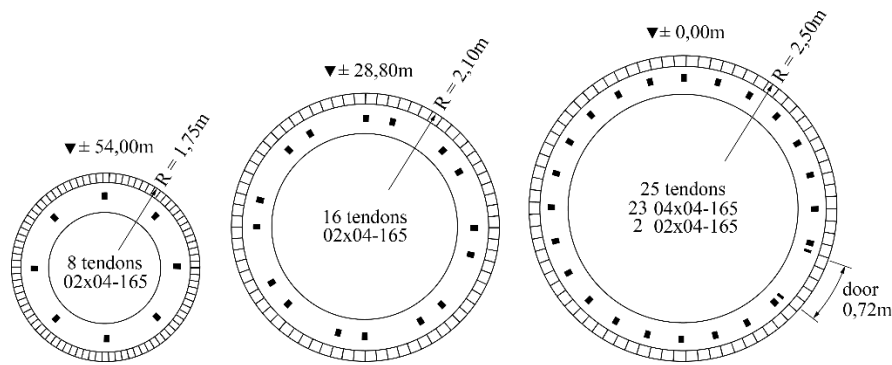
Figure 7. Distribution of tendons in representative cross sections of the tower.

The maximum compressive stresses were determined under the quasi-static load combination DLC 1.6, Table 5. The limitation was chosen to be the fatigue reference compressive strength of concrete determined with Eq. (5) from [21]. This choice was made due to the unforeseeable occurrence of the maximum load cycles. The maximum compressive stress may also occur late in the structure's service life, while the resistance of the load-bearing structure is reduced due to a weakening from dynamic actions. By selecting the fatigue reference compressive strength as the upper limit for the compression stresses in ULS, a conservative estimation of the load bearing capacity of the concrete construction takes place.

$$f_{cd,fat} = 0.85 \cdot \frac{f_{ck}}{\gamma_C} \cdot \left(1 - \frac{f_{ck}}{400\ \text{MPa}}\right) \tag{5}$$

Table 7: Design internal forces and verification for ULS based on the results of the global analysis [7]

	Bending moment	Required prestressing force	Number of tendons	Prestressing force	Stress state in concrete
	M [kNm]	P_{m0} [kN]	notations	P_{m0} ($P_{m\infty}$) [kN]	σ_{cd} [MPa]
72,00m — 54,00m	2645 — 11195	3318 — 14082	8 VT-CMM KD 04x02 - 165	14000 (12250)	33 — 43 ; $f_{cd,ULS}$ = 65
54,00m — 28,80m	11195 — 26136	14082 — 27642	16 VT-CMM KD 04x02 - 165	28000 (24500)	40 — 43 ; $f_{cd,ULS}$ = 65
28,80m — 0,00m	26136 — 47295	27642 — 40926	23 VT-CMM KD 04x02 - 165 2 VT-CMM KD 02x02 - 165	42000 (35900)	43 — 43 ; $f_{cd,ULS}$ = 65

The whole structure was checked in the global analysis; the individual segments were also proven to satisfy the requirements for strength, deformability and cracking. The calculation was carried out by means of maximum stresses in the concrete under load and compared with the design values. The maximum compression stress was detected for the 8th segment from the base up, where the first set of tendons are anchored, Fig. 8. This value of 46 MPa (Fig. 8 and 9) is slightly higher than the value of 43 MPa obtained by the global analysis (Table 7). The difference is due to the local effect of the eccentrically anchored tendons, which causes an additional bending moment in the wall segment (Fig. 3). Moreover, the magnitude of the additional bending moment was drastically reduced due to the ring beam in the upper part of the segment which was included as part of the model for the local analysis. The maximum compressive stresses are below the fatigue reference strength $f_{cd,fat}$ = 65 MPa, which means that the compressive strength requirements in the ULS are fulfilled.
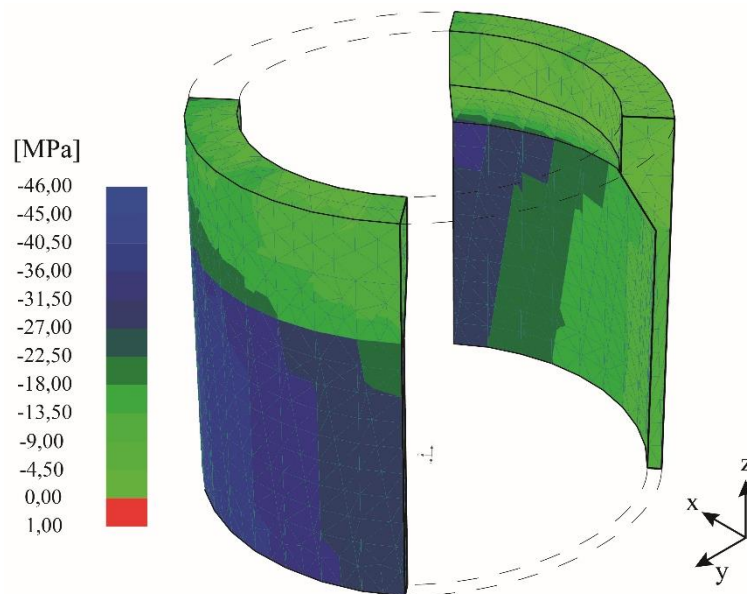
Figure 8. The normal stresses σ_{zz} distribution in the 8th segment corresponding the ULS, as a result of the FEA with software ATENA 3D.

Knowledge about the long-term tensile strength of UHPFRC is still modest and needs to be deepened through more studies. Based on his tests, Rinder [22] reported a tensile strength of 85 % for unreinforced high-strength concrete (HSC) under long-term loads, while Han and Walraven [23] stated a percentage of 75 %. Task Group 8.6 [24] estimated a long-term tensile strength of 90 % of the short-term tensile strength for UHPFRC [3]. Based on this data, a presumptive coefficient α_{ct} = 0,9 was used from [3], which needs to be validated in further research projects. The design tensile strength of UHPFRC was determined with Eq. (6) in the case of no orientated fibers, and with Eq. (7) when all fibers are orientated parallel to the direction of the tensile stresses. Applying these two equations and using the characteristic tensile strength of the concrete exposed in Table 1, the design values $f_{ctd,el}$ = 5,3 MPa and $f_{ctd,1D,el}$ = 15,7 MPa were obtained.

$$f_{ctd,el} = \alpha_{ct} \cdot \frac{f_{ctk,el}}{\gamma_C} \tag{6}$$

$$f_{ctd,1D,el} = \alpha_{ct} \cdot \frac{f_{ctk,1D,el}}{\gamma_C} \tag{7}$$

In the ULS, the tensile stresses spread in the x-direction over a large area in the middle part of the segment (Fig. 9). The cause of the tensile stresses is the temperature difference of 15 K applied between the positive and negative side in the x-direction. The maximum tensile stresses in the tower structure reach magnitudes of 6,50 MPa, which is above the design tensile strength of UHPFRC without fiber orientation $f_{ctd,el}$. Furthermore, when the fiber orientation procedure was applied, the design tensile strength $f_{ctd,1D,el}$ became twice as large as the maximum tensile stresses.
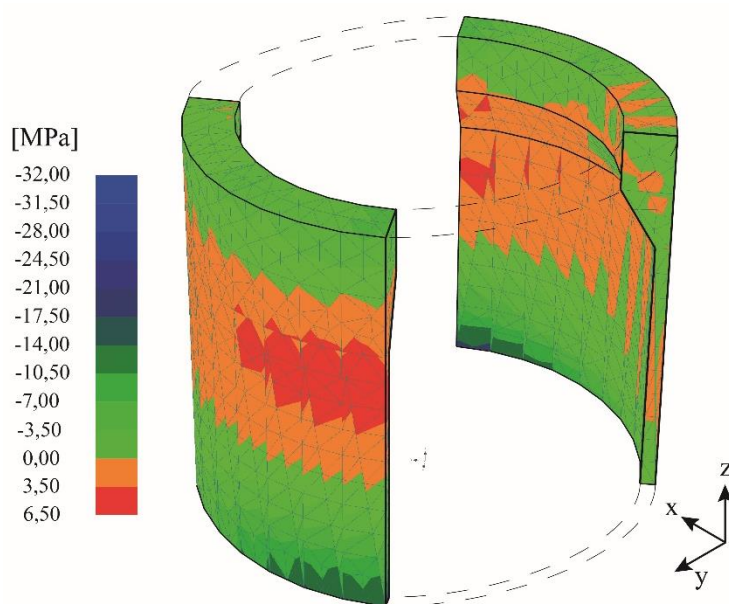
Figure 9. The normal stresses σ_{xx} distribution in the 8th segment corresponding the ULS, as a result of the FEA with software ATENA 3D.

Both the compression and tensile strains in the concrete segments were compared with the maximum strains for the UHPFRC utilised. Eq. (8) was used to check the compression strains and Eq. (9) to check the tensile strains. Due to insufficient information about the loads in the serviceability limit state (SLS), the loads from the ULS were considered as a conservative measure for the checking. The verification was considered to be complied when the FEA results showed maximum compressive strains smaller than ε_{c1} and maximum tensile strains not exceeding the corresponding tensile elasticity limit $\varepsilon_{ct,el}$ of the UHPFRC. This way, it was ensured that no cracks will appear in the concrete cross section.

$$\varepsilon_{cd} \leq \varepsilon_{c1} \tag{8}$$

$$\varepsilon_{ctd} \leq \varepsilon_{ct,el} \tag{9}$$

The strain distributions in the three directions of the Cartesian axes are shown in Figure 10, being exemplified on the relevant segment of the tower as a result of the nonlinear analysis. In the x-direction appear positive strains (specific to tensile stresses) of up to 0,25 ‰. Firstly because of the temperature load and secondly due to the prestressing forces acting eccentrically. The strains are exceeding $\varepsilon_{ct,el} = 0,19$ ‰ and, as a result, a few vertical cracks appear in these regions. As for the negative strains, the maximum value -0,38 ‰ is ten times smaller than ε_{c1}. In the y-direction, there is a situation similar to ε_{xx} distribution with tensile strains exceeding the $\varepsilon_{ct,el}$. The maximum value is 0,62 ‰ and it is caused by the large influence of the temperature load. Consequently, vertical cracks with the maximum opening appear in this region. However, the maximum compression strains of -0,41 ‰ can be easily taken by the UHPFRC. The strains distribution in the z-direction corresponds exactly to the σ_{zz} profile (Figure 8). The entire cross section is under compressive

strains of up to -0,85 ‰. The proof is fulfilled once again by virtue of UHPFRC with ε_{c1} = -4,00 ‰.
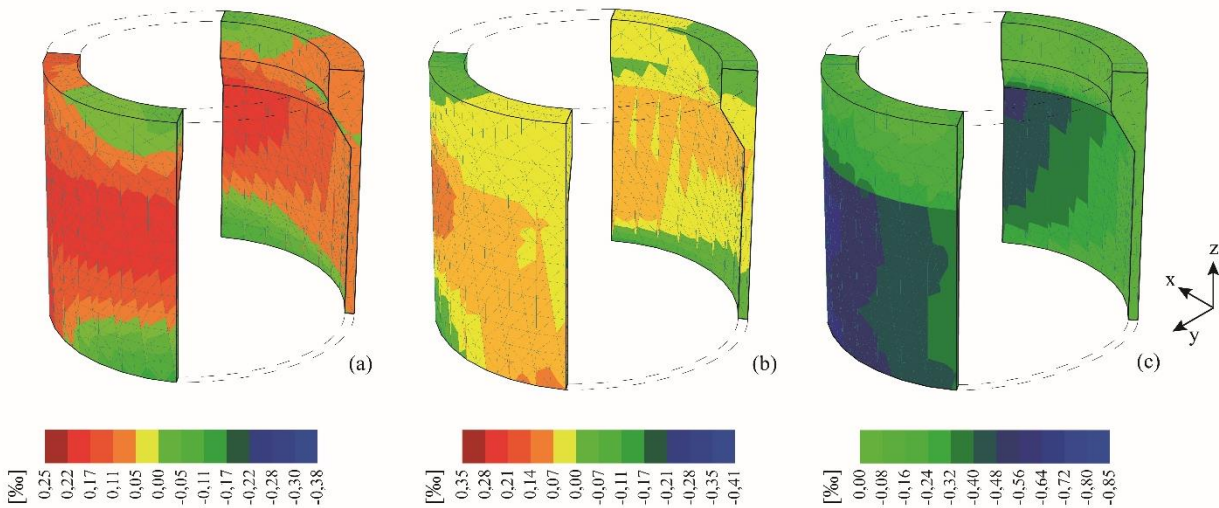
Figure 10. The strains ε_{xx} (a), ε_{yy} (b) and ε_{zz} (c) distribution in the 8th segment corresponding the ULS, as a result of the FEA with software ATENA 3D.

4.3 Fatigue limit state (FLS)

The FLS can also be considered as a special case of ULS. Here, a component failure occurs due to the accumulation of damage during changing stresses [20]. In addition to the strength of the concrete, the expected number of load cycles N is also decisive for the fatigue check. The limit for the compression strength of concrete can be determined depending on the load profiles. A simplified proof is proposed in [5] for a nominal number of cycles $N_{nom} < 2 \cdot 10^9$. In the case of the present WT, a maximum number of load cycles, $N = 5,3 \cdot 10^8$ is to be expected [7]. So using Eq. (10), one can determine the maximum concrete compression stress permissible in the FLS. The stress distribution in the ring cross-section of the tower is illustrated in Figure 11.

$$S_{cd,max} \leq 0,40 + 0,46 \cdot S_{cd,min} \tag{10}$$

in this case

$$S_{cd,min} = \gamma_{Sd} \cdot \sigma_{c,min} \cdot \eta_c / f_{cd,fat}$$

$$S_{cd,max} = \gamma_{Sd} \cdot \sigma_{c,max} \cdot \eta_c / f_{cd,fat}$$

$$\eta_c = \frac{1}{1,5 - 0,5 \cdot \frac{\sigma_{c1}}{\sigma_{c2}}}$$
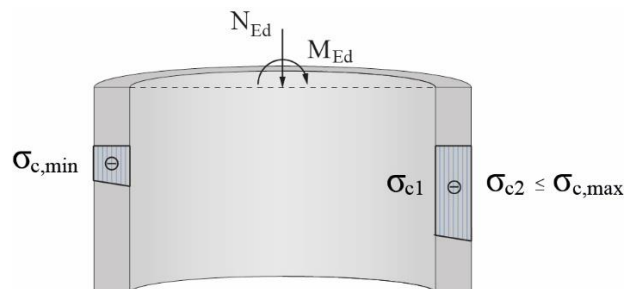
Figure 11. The normal stresses diagram in the tower shaft for calculating η_c [5].

The FEA results for the global model in the FLS (Table 8) point out that the necessary prestress force $P_{m\infty}$ is slightly smaller in each section than what is required in the ULS (Table 7). Consequently, the quantity and size of the tendons is determined by the stress state corresponding to the ULS load cases. In order to consider the fatigue effect upon the tendon strength, Eq. (11) was used with respect to the indications in [25].

$$\gamma_{Sd} \cdot \max \Delta\sigma_{Ss} \leq \frac{\Delta\sigma_{Rsk}}{\gamma_{s,fat}} \tag{11}$$

The maximum stress variation results from the fatigue bending moment ΔM_{fat} and depends on the tower height. The stress resistance $\Delta R_{sk}(n)$ can be graphically determined for tension members according to [25], Figure 12. A maximum stress variation resistance of 85 MPa corresponds to the current design number of cycles $N = 5{,}3 \cdot 10^8$. The tendons were checked with the present value for fatigue and no failure occurred over the entire height. By and large, the tower structure checking is validated also for the FLS.
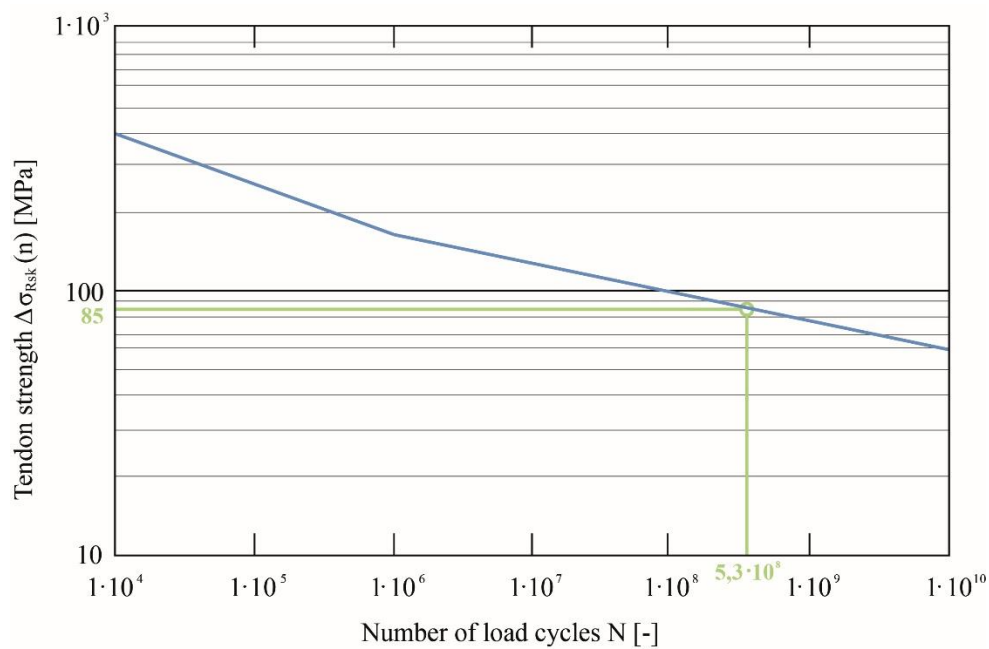
Figure 12. The normal stresses diagram in the tower shaft for calculating η_c [5].

The further results of the FEA show a range between 25 and 30 MPa for the concrete maximum compression stresses along the tower height, lower than the allowed concrete strength $\sigma_{c,max} = 32$ MPa (Table 8). The local FEA of an individual segment (Figure 13) shows a maximum compression stress of 33 MPa, an increased value compared to the one obtained by the global analysis. The difference between the two results is the consideration of the tendon eccentricity. In the global analysis, the local stress state and deformation of the segments in the corbel region were neglected, so the prestress force was defined as a centrically applied compression force. Furthermore, in the local analysis the prestress force was applied eccentrically in relation to the wall segment. Consequently, the maximum compression stress in the FLS is slightly higher than the concrete strength $\sigma_{c,max}$, while the maximum concrete tensile stress is nearly zero. It can be stated that the material is being efficiently used due to the high degree of utilisation.

Table 8: Design internal forces and verification for FLS based on the results of the global analysis [7]

	Bending moment	Required prestressing force	Number of tendons	Prestressing force	Stress state in concrete
	M [kNm]	P_{m0} [kN]	notations	P_{m0} $(P_{m\infty})$ [kN]	σ_c [MPa]
72,00m / 54,00m	148 ... 1082	3318 ... 14082	8 VT-CMM KD 04x02 - 165	14000 (12250)	27 ... 25 ($\sigma_{c,max}$ = 32)
54,00m / 28,80m	1082 ... 4749	14082 ... 27642	16 VT-CMM KD 04x02 - 165	28000 (24500)	29 ... 27 ($\sigma_{c,max}$ = 32)
28,80m / 0,00m	4749 ... 11694	27642 ... 40926	23 VT-CMM KD 04x02 - 165; 2 VT-CMM KD 02x02 - 165	42000 (35900)	30 ... 28 ($\sigma_{c,max}$ = 32)
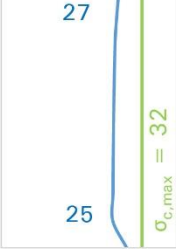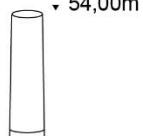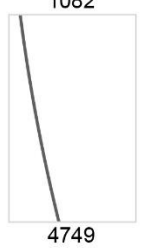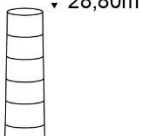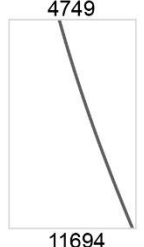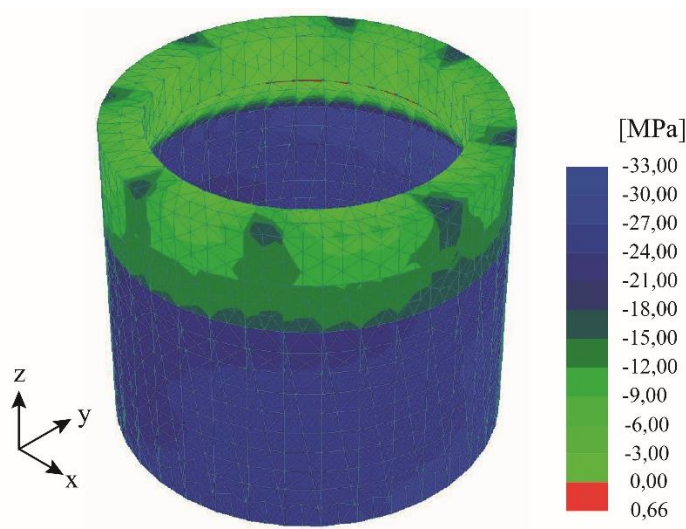
Figure 13. The normal stresses σ_{zz} distribution in the 8th segment corresponding the FLS, as a result of the FEA with software ATENA 3D.

5. Conclusions

The research results presented in this paper confirm the high potential of a segmented tower structure made of UHPFRC for onshore wind turbines. A design approach on the basis of the eigenfrequency analysis allows the pre-dimensioning of the tower geometry made of UHPFRC with a truncated conic shape in the hypothesis of closed joints. This works similar to a monolithic structure without a stiffness reduction caused by the segmentation, independent of the external conditions. The most relevant factors were considered in the tower dimensioning, such as: site-specific conditions, wind effects and operating loads from wind turbines. Using nonlinear static and dynamic analysis, the tower structure could be further optimized. The results of the numerical investigations show the possibility of building a 72 m tower with only 130 m^3 of concrete. The material consumption is reduced to half compared to a prestressed concrete tower cast in situ [18]. Moreover, the solution brings secondary advantages as simplicity by erecting the tower and later on by disassembling and recycling it.

Notations

$f_{cd,fat}$	design fatigue reference strength of concrete under compression
f_{ck}	characteristic compressive cylinder strength of concrete at 28 days
$f_{ctk,el}$	characteristic axial tensile strength of concrete when the elasticity limit is reached
f_E	blade passing frequency
f_R	rotor frequency
f_1	first eigenfrequency
fib	Fédération Internationale du Beton
k_u	foundation replacement spring stiffness for translation
k_φ	foundation replacement spring stiffness for rotation
r_0	foundation radius, in plane
A	accidental
A_{cs}	cross sectional area
DLC	design load case
E_{cm}	Secant modulus of elasticity of concrete
ECG	extreme coherent gust
ECD	extreme coherent gust with change of direction
EDC_1	extreme wind direction change for 1-year return period
EDC_{50}	extreme wind direction change for 50-year return period
EOG_1	extreme operating gust for 1-year return period
EOG_{50}	extreme operating gust for 50-year return period
EWM	extreme wind speed model
EWS	extreme wind shear
F	fatigue
FEA	finite element analysis

FLS	fatigue limit state
G_d	dynamic shear modulus for soil
K	Kelvin (unit measure for temperature)
$\overline{K}$	stiffness matrix
M_{Ed}	design value of the applied bending moment
$\overline{M}$	total mass
N	normal and extreme
N_{Ed}	design value of the applied axial force
NTM	normal turbulence model
NWP	normal wind profile model
$S_{cd,max}$	maximum effective concrete compressive stress in the FLS
$S_{cd,min}$	minimum effective concrete compressive stress in the FLS
T	transport and erection
UHPFRC	ultra-high performance fiber reinforced concrete
ULS	ultimate limit state
W	section modulus
1P	periodic excitation with 1 x rotational speed (rotor frequency)
3P	periodic excitation with 3 x rotational speed from blade passing frequency
α_{ct}	coefficient taking into account long term effects on the tensile strength and of unfavorable effects
ΔM_{II}	additional bending moment due to the second order effect
ΔM_{fat}	maximum variation of bending moments values in FLS
$\Delta \sigma_{Rsk}$	stress range relevant to N cycles obtained from a characteristic fatigue function
ε_{ctd} [‰]	design tensile strain
$\varepsilon_{ct,el}$ [‰]	tensile strain in the concrete corresponding the tensile elasticity limit of UHPFRC
ε_{cd} [‰]	design compressive strain
ε_{c1} [‰]	compressive strain in the concrete at the peak stress f_{cm}
η_c	factor for taking into account the non-uniform distribution of the concrete compressive stresses in one cross section
γ_C	partial factor for concrete
γ_P	partial safety factor for actions associated with prestressing
γ_{Sd}	partial safety factor for modeling inaccuracies in the stress calculation (1.10)
$\gamma_{s,fat}$	partial safety factor for the material properties of reinforcing and prestressing steel under fatigue loading (1.15)
ω_i	the "i" natural frequency of the multi-mass oscillator model
v	Poisson ratio for soil
$\sigma_{cd,max}$	maximum concrete compressive stress
$\sigma_{cd,min}$	minimum concrete compressive stress at the same point at which $\sigma_{cd,max}$ occurs, calculated for the lower value of the action (used $\sigma_{cd,min} = 0$ for tensile stresses)
σ_{Ed}	design value of the compressive stress in the concrete
σ_{Ss}	steel stress range under acting loads

6. References

[1] Bundesanzeiger. Bekanntmachung - Forschungsförderung im 6. Energieforschungsprogramm "Forschung für eine umweltschonende, zuverlässige und bezahlbare Energieversorgung, *Hrsg. Bundesministerium für Justiz und Verbraucherschutz*, Berlin 2014.

[2] Rebelo C, Moura A, Gervásio H, Veljkovic M, Simões da Silva L. Comparative life cycle assessment of tubular wind towers and foundations – Part 1: Structural design. *Engineering Structures*, Elsevier Ltd. **Vol. 74**, pp. 289-291, 2014.

[3] Plank M, Frettlöhr B, Quappen J, Sobek W. *Strukturoptimierte Türme für Offshore - Windenergieanlagen aus UHFFB in Segmentbauweise: Abschlussbericht zum Forschungsvorhaben SF-10.08.18-7-09.25; II3-F20-09-43 der Forschungsinitiative "Zukunft Bau"*. Institut für Leichtbau Entwerfen und Konstruieren (ILEK), Universität Stuttgart, 2014.

[4] Wefer M. *Materialverhalten und Bemessungswerte von ultrahochfestem Beton unter einaxialer Ermüdungsbeanspruchung*. Berichte aus dem Institut für Baustoffe, Heft 7 (Institut für Baustoffe, Leibniz Universität Hannover), 2010.

[5] Grünberg J, Göhlmann J. Concrete Structures for Wind Turbines. *Beton-Kalender*, Wilhelm Ernst &h Sohn, Berlin, Germany, 2013.

[6] Grünberg J, Göhlmann J. Tragwerksplanung von Windenergieanlagen in Spannbetonbauweise [Structural design of prestressed concrete wind turbine structures]. *Der Bauingenieur*, Springer VDI Verlag. **Vol. 10**, pp. 441-449, 2008.

[7] Konzept Bau Bühl: Transport von Fertigteilen.
URL: http://vh.bfwbausuedbaden.de/files/3/73/74/1.42 TransportvonBauelementen.pdf [accessed on 2014-04-11], 2011.a

[8] Anger J, Bange J, Blick C, Brosz F, Emeis S, Fallmann J, Felder M, Haase W, Heckelsmüller G, Kaifel A, Kalisch K, Kern S, Kim Y, Kudella P, Lemmer F, Lipp A, Lutz T, Quénéhervé G, Rautenberg A, Rettenmeier A, Sayed M, Schmeer D, Schmölz M, Schöbel S, Schulz C, Sehnke F, Simisker M, Toader N, Triantafafyllidis T, Westermann K, Wüchner R. *Erstellung einer Konzeption eines Windenergie-Testgeländes in bergig komplexem Terrain (KonTest)*. Abschlussbericht des Forschungsprojektes 0325656 A-D, 2016.

[9] Germanischer Lloyd: *Richtlinie für die Zertifizierung von Windenergieanlagen*, Hamburg 2007.

[10] Gasch R, Twele J. *Windkraftanlagen - Grundlagen, Entwurf, Planung und Betrieb*. 6. Auflage. Hrsg. Teubner, Wiesbaden 2010.

[11] Sobek W, Plank M, Frettlöhr B, Röhm J, Corvez D. *RILEM-fib-AFGC Int. Symposium on Ultra-High Performance Fibre-Reinforced Concrete*. Marseille, France, 2013.

[12] Kühn M. *Dynamics and Design Optimisation of Offshore Wind Energy Conversion Systems*, Report 2011.002, 2nd edition (DUWIND – Delft University Wind Energy Research Institute, Delft), 2003.

[13] Van der Tempel J, Molennar D sP. *Soft-Soft, not hard enough?*, Proceedings of the World Wind Energy Conference, Berlin, 2002.

[14] Technical data of the wind turbine FL 600/75, Fuhrländer, 2008.

[15] Schaumann P, Seidel M. *Weiterentwicklung der Verfahren zur sicheren und wirtschaftlichen Bemessung von Türmen für Windkraftanlagen mit hoher Leistung*. Schriftenreihe Heft 18; Institut für Stahlbau, Universität Hannover, 1999.

[16] Empfehlungen der Arbeitskreises 1.4 "Baugrunddynamik" der Deutschen Gesellschaft für Geotechnik (DGGV). *E 3 Federsteifigkeiten und Dämpfung starrer Fundamente auf dem Baugrund*. Bautechnik (75) 10, 792-805, 1998.

[17] Petersen C. *Dynamik der Baukonstruktion*. Hrsg. Vieweg & Sohn, Braunschweig/Wiesbaden 1996.

[18] Engström S, Lyrner T, Hassanzadeh M, Stalin T, Johansson J. *Tall towers for large wind turbines*. Report from Vindforsk project V-342 Höga torn för vindkraftverk. Elforsk rapport 10:48, 2010.

[19] Deutsches Institut für Bautechnik (DIBt). *Richtlinie Windenergieanlagen. Einwirkungen und Standsicherheitsnachweise für Turm und Gründung (wind turbines guideline – actions on and stability analyses for tower and foundation)*. Berlin, 2004.

[20] Zilch K, Zehetmaier G. *Bemessung im konstruktiven Betonbau: Nach DIN 1045-1 und DIN EN 1992-1-1*, 2. Aufl. Berlin, Heidelberg: Springer, 2010.

[21] International Federation for StructuralConcrete (fib). *Model code 2010 Volume 1: Final draft*. Lausanne, Switzerland, 2012.

[22] Rinder T. *Hochfester Beton unter Dauerzuglast*. DAfStb Heft 544. Beuth Verlag, Berlin, 2003.

[23] Han N, Walraven J C. *Sustained loading effects in high strength concrete*. In: Holand, I.; Sellevold, E. (Hrsg.): Proceedings High-Strength Concrete, Lillehammer, **Vol. 2**, pp. 1076-1083, 1993.

[24] Fédération Internationale du Beton – fib-TG 8.6 (2010): *Recommendations for Ultra High Performance Fibre Reinforced Concrete - UHPFRC*. Draft (2010) of Taskgroup 8.6, fib, 2010.

[25] International Federation for StructuralConcrete (fib). *Model code 2010 Volume 2: Final draft*. Lausanne, Switzerland, 2012.